INAF
ISTITUTO NAZIONALE
DI ASTROFISICA
NATIONAL INSTITUTE
FOR ASTROPHYSICS

Publication Year	2016
Acceptance in OA@INAF	2020-06-17T09:42:33Z
Title	þÿ S i z e - f r e q u e n c y d i s t r i b u t i o n o f b o u l d e r s "e 1 0 m o n c o m
Authors	PAJOLA, MAURIZIO; LUCCHETTI, ALICE; BERTINI, IVANO; MARZARI, FRANCESCO; A'Hearn, Michael F.; et al.
DOI	10.1051/0004-6361/201526834
Handle	http://hdl.handle.net/20.500.12386/26097
Journal	ASTRONOMY & ASTROPHYSICS
Number	585

A&A 585, A85 (2016)
DOI: 10.1051/0004-6361/201526834
© ESO 2015

Astronomy & Astrophysics

Size-frequency distribution of boulders ≥10 m on comet 103P/Hartley 2

Maurizio Pajola[1,2], Alice Lucchetti[1,3], Ivano Bertini[1], Francesco Marzari[4], Michael F. A'Hearn[5], Fiorangela La Forgia[4], Monica Lazzarin[4], Giampiero Naletto[6,7], and Cesare Barbieri[1,4]

[1] Center of Studies and Activities for Space, CISAS, "G. Colombo", University of Padova, via Venezia 15, 35131 Padova, Italy
e-mail: maurizio.pajola@gmail.com, maurizio.pajola@unipd.it
[2] NASA Ames Research Center, Moffett Field, CA 94035, USA
e-mail: maurizio.pajola@nasa.gov
[3] INAF–Astronomical Observatory of Padova, Vicolo dell'Osservatorio 5, 35131 Padova, Italy
[4] Department of Physics and Astronomy "G. Galilei", University of Padova, Vic. Osservatorio 3, 35122 Padova, Italy
[5] Department for Astronomy, University of Maryland, College Park, MD 20742-2421, USA
[6] Department of Information Engineering, University of Padova, via Gradenigo 6/B, 35131 Padova, Italy
[7] CNR-IFN UOS Padova LUXOR, via Trasea 7, 35131 Padova, Italy

Received 25 June 2015 / Accepted 11 November 2015

ABSTRACT

Aims. We derive the size-frequency distribution of boulders on comet 103P/Hartley 2, which are computed from the images taken by the Deep Impact/HRI-V imaging system. We indicate the possible physical processes that lead to these boulder size distributions.
Methods. We used images acquired by the High Resolution Imager-Visible CCD camera on 4 November 2010. Boulders ≥10 m were identified and manually extracted from the datasets with the software ArcGIS. We derived the global size-frequency distribution of the illuminated side of the comet (∼50%) and identified the power-law indexes characterizing the two lobes of 103P. The three-pixel sampling detection, together with the shadowing of the surface, enables unequivocally detection of boulders scattered all over the illuminated surface.
Results. We identify 332 boulders ≥10 m on the imaged surface of the comet, with a global number density of nearly 140/km^2 and a cumulative size-frequency distribution represented by a power law with index of −2.7 ± 0.2. The two lobes of 103P show similar indexes, i.e., −2.7 ± 0.2 for the bigger lobe (called L1) and −2.6 +0.2/ − 0.5 for the smaller lobe (called L2). The similar power-law indexes and similar maximum boulder sizes derived for the two lobes both point toward a similar fracturing/disintegration phenomena of the boulders as well as similar lifting processes that may occur in L1 and L2. The difference in the number of boulders per km^2 between L1 and L2 suggests that the more diffuse H_2O sublimation on L1 produce twice the boulders per km^2 with respect to those produced on L2 (primary activity CO_2 driven). The 103P comet has a lower global power-law index (−2.7 vs. −3.6) with respect to 67P. The global differences between the two comets' activities, coupled with a completely different surface geomorphology, make 103P hardly comparable to 67P. A shape distribution analysis of boulders ≥30 m performed on 103P suggests that the cometary boulders show more elongated shapes when compared to collisional laboratory fragments as well as to the boulders present on the surfaces of 25 143 Itokawa and 433 Eros asteroids. Consequently, this supports the interpretation that cometary boulders have different origins with respect to the impact-related asteroidal boulders.

Key words. comets: general – comets: individual: 103P/Hartley 2 – methods: data analysis

1. Introduction

On 4 November 2010, NASA Deep Impact flyby spacecraft/EPOXI[1] spacecraft flew by the Jupiter-family comet 103P/Hartley 2 (hereafter 103P) at 1.06 AU from the Sun and 0.16 AU from the Earth.

The Deep Impact High Resolution Instrument (HRI), consists of a long focal length telescope (10.5 m) with an aperture diameter of 30 cm (Klaasen et al. 2008). A dichroic beam splitter is located in front of the focal plane, reflecting visible light (0.3 to 1.0 μm) through a filter wheel to a CCD for direct imaging and transmitting near-infrared (1.0 to 5.0 μm) to a 2-prism spectrometer. The visible instrument is called High Resolution Imager – Visible (HRI-V) and its filter wheel has two clear apertures and seven filters centered at 0.45, 0.55, 0.65, 0.75, and 0.85 μm. The IR instrument is called the High Resolution IR spectrometer (HIRI-IR). The HRI-V has a spatial scale of 1.4 m/px when it is at 700 km from the surface. Since 5 September 2010, multiple observations of 103P have been performed by using all EPOXI instruments. The entire HRI-V 103P dataset consists of 10^5 1024 × 1024 px^2 images.

The description of the nucleus properties and its activity, as observed by HRI-V, HRI-IR, and the Medium Resolution Instrument (MRI) is presented in A'Hearn et al. (2011). The 103P is a Jupiter-family comet that completes an orbit around the Sun in 6.46 years. It has a complex excited state of rotation showing a roll around the long axis with period of 27.79 (or 55.42) ±0.1 h, accompanied by a precession of the same axis around the angular momentum vector with a period of 18.34 ± 0.04 h (A'Hearn et al. 2011). 103P is characterized by a bigger lobe, hereafter called L1, and a smaller lobe, hereafter

[1] After observing and analyzing the comet 9P/Tempel 1 (A'Hearn et al. 2005), the Deep Impact mission was redirected to comet 103P/Hartley 2 as part of an extended mission named EPOXI, i.e., Extrasolar Planet Observation and deep impact eXtended Investigation. Therefore, this EPOXI acronym refers to the Deep Impact extended mission.

called L2, connected by a so-called waist region. This bilobed shape has a maximum length of 2.33 km and a mean radius of 0.58 ± 0.02 km. The total area of the comet derived through the shape model is 5.24 km^2. The EPOXI flyby did not allow the measurement of the mass of the comet, nonetheless, with a measured volume of 0.81 ± 0.08 km^3, and by assuming that the surface of the waist was an equipotential, the density was estimated to be 300 kg/m^3 (Thomas et al. 2013).

103P is a hyperactive comet with an active fraction (area based on Q_{H_2O}/area of the nucleus) near 1.7–2.5 (Kelley et al. 2013), i.e., about the double of the actual nucleus surface should be required to account for the total production rate of this comet. The presence of an icy grains halo was suggested to explain this high activity (Lisse et al. 2009), which increased the surface area available for sublimation and the relatively high water production rate. Images obtained during the flyby showed a coma of large particles reaching dimensions between 0.1 and 2.21 m, with a few of the largest particles reaching effective radii close to 4 m (Kelley et al. 2013), surrounding the nucleus (A'Hearn et al. 2011). These individual large chunks move at 0.5–2 m s^{-1} and had already been detected via radar observations just before the close encounter (Harmon et al. 2011). The largest chunks detected from the spacecraft were icy, and dragged from the nucleus with escaping carbon dioxide into the coma: their sublimation provides a large fraction of the total H_2O gaseous output of the comet (A'Hearn et al. 2011).

Near-IR spectra of 103P were acquired for several weeks before and after closest approach (the closest approach, hereafter shortened with CA, occurred with a maximum HRI-IR spatial resolution of 7 m/pixel) and two significant volatile species, H_2O (2.7 μm) and CO_2 (4.3 μm), were the dominant emission bands detected in spectra. At the CA, the distribution of these parent species was found to be highly asymmetric showing that CO_2 and H_2O have different source regions (A'Hearn et al. 2011; Protopapa et al. 2014). In particular, EPOXI observations revealed that a water vapor-rich region extended roughly perpendicular to the waist of the nucleus with a little content of CO_2 and lack of water ice, while the CO_2 was concentrated in jets that occurred at both ends of the comet with the strongest activity centered on the L2 end. The distribution of water ice grains is correlated with CO_2 jets, suggesting that CO_2 rather than H_2O drags water ice grains with it into the coma as it leaves the nucleus (A'Hearn et al. 2011).

In this work, we focus on the positive relief located on knobby terrains of 103P and measure the size-frequency distribution of what we call boulders. This terminology is not meant to imply any structural similarity to the boulders normally seen on Earth. The paper is organized as follows: in Sect. 2, we provide the dataset and methodology used in this analysis; in Sect. 3 we give the results regarding the boulder size-frequency distribution found on 103P, while in Sect. 4 we report on the interpretation of the results and discuss them in the context of what it has been already analyzed on the 67P/Churyumov-Gerasimenko comet.

2. Dataset and methodology

On 4 November 2010, i.e., one week after perihelion passage, Deep Impact/EPOXI spacecraft flew by comet 103P. The CA occurred at a distance of 694 km from the comet center at 13:59:47 UT, 1.064 AU from the Sun and 0.156 AU from the Earth. The spacecraft speed was 12.3 km s^{-1}. During the CA, full-frame (1024 × 1024 px^2) HRI-V images of the nucleus with spatial scale ranging from 5 to 2 m/px have been obtained. This dataset is of extreme importance to study in detail the surface properties of the nucleus and to understand the geology of the comet.

As presented in A'Hearn et al. (2011) and confirmed in Thomas et al. (2013), the knobby terrains of 103P show the presence of rounded to angular elevated forms, also called mounds (Thomas et al. 2013), which reach, in a few cases, up to 50 m height and 70 m width. We therefore focused our attention on these positive reliefs to understand if they presented any possible boulder-like, size-frequency distribution.

We define as boulder a positive relief detectable in different images with the constant presence of an elongated shadow (if the phase angle is higher than 0°)[2] whose extension depends on the illumination geometry; see Fig. 1 for an explanation; in addition, a boulder seems to be detached from the ground where it stands. Assuming that the mounds presented in Thomas et al. (2013) can be considered boulders located on the comet surface, we extended the previous database and double checked the 103P positive reliefs by making use of 3D analgyphs specifically prepared for this purpose; see, e.g., Fig. 2.

The dataset we used to derive the cumulative size-frequency distribution of the 103P boulders is presented in Table 1. All the selected images were taken with the CLEAR 1[3] filter at 0.65 μm. We made use of the public Planetary Data System images[4] deconvolved as described in Lindler et al. (2013). Moreover, by following Lindler et al. (2013), we considered only those that are present in multiple images to be real positive reliefs in order not to be affected by the noise amplification and ringing[5]. As a result of the slight difference in resolution (2.8–3.9 m) between the images used in this work, we considered as statistical meaningful those detections with a diameter larger than 10 m. This value is above the 8.4 m, corresponding to the three-pixel sampling rule (Nyquist 1928) derived from the highest resolution images, but below the 11.7 m three-pixel sampling value forced by the first, lower resolution image. Nonetheless, as will be clear in the analysis, the majority of the boulders (91%) are identified in the three highest resolution images, which enable a clear identification of boulders larger than 10 m. Therefore, we believe that the value of 10 m can be considered the lower limit of our global boulder detection.

[2] Since the observations were performed with an average phase angle of 86°, the presence of elongated shadows on the surface provides the possibility of identifying even smaller boulders (two pixels in diameter, ~6–9 m). However, we decided to exclude these smaller boulders in the cumulative size-frequency distribution because their statistics cannot be considered complete because of the resolution limit.

[3] The 0.65 μm filter, called CLEAR 1 filter, has a full width at half maximum ($FWHM$) > 700 nm, made of uncoated fused silica and not band limited (Klaasen et al. 2008).

[4] PDS reference: Lindler, D.J., M.F. A'Hearn, and S.A. McLaughlin, EPOXI 103P/HARTLEY2 ENCOUNTER – HRIV DECONVOLVED IMGS V1.0, DIF-C-HRIV-5-EPOXI-HARTLEY2-DECONV-V1.0, NASA Planetary Data System, 2012.

[5] The EPOXI High Resolution Instrument, HRI, was found to be out of focus after launch (Klaasen et al. 2008), therefore, deconvolution technique was applied to restore some of cometary nucleus images (Lindler et al. 2013). A set of deconvolved images was included in Planetary Data System, but it should be considered that the deconvolution processing often introduces artifacts that complicate their use in geological interpretation. Guidelines explained in Lindler et al. (2013) should be used to correctly interpret the results coming from these deconvolved images, for example it is known that features coming from noise amplification or unmasked detector defects will not repeat between images. Since boulders are visible in different images with different scales, we consider these features as real and not a product of the restoration algorithm.

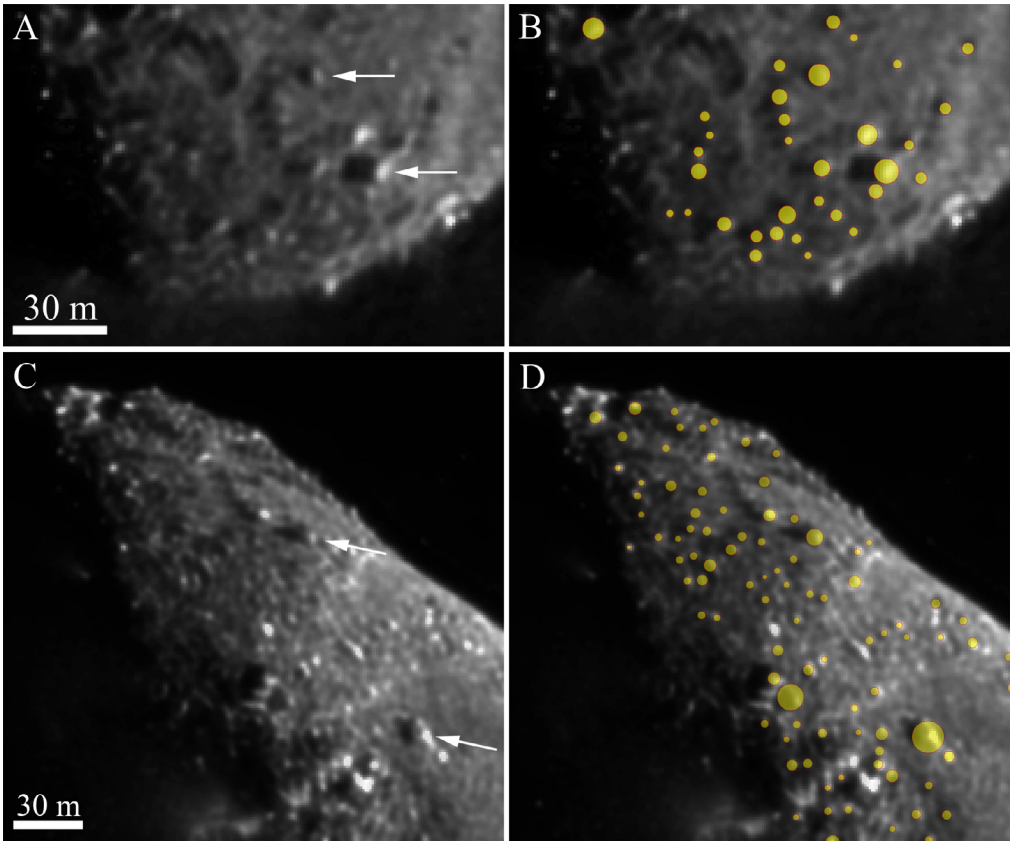

Fig. 1. Example of the methodology used to identify the boulders on the surface of 103P. **A)** Subframe of a HRI-V image (HV10110413-5004015-001) taken on 4 November 2010 at a distance of 1416.4 km from the surface of 103P. The scale of the image is 2.83 m/px. The white arrows indicate the direction of the solar irradiation. In this figure, the shadows of the boulders are observable on the left of such positive reliefs. **B)** The same image with the detected boulders indicated in yellow circles are presented. **C)** Subframe of a HRI-V image (HV10110414-5006002-001) taken on 4 November 2010 at a distance of 1407.2 km from the surface of 103P. The scale of the image is 2.81 m/px. The white arrows indicate the direction of the solar irradiation. As from the above image, the shadows of the boulders are observable on the left of the positive reliefs. **D)** The same image with the detected boulders indicated in yellow circles.

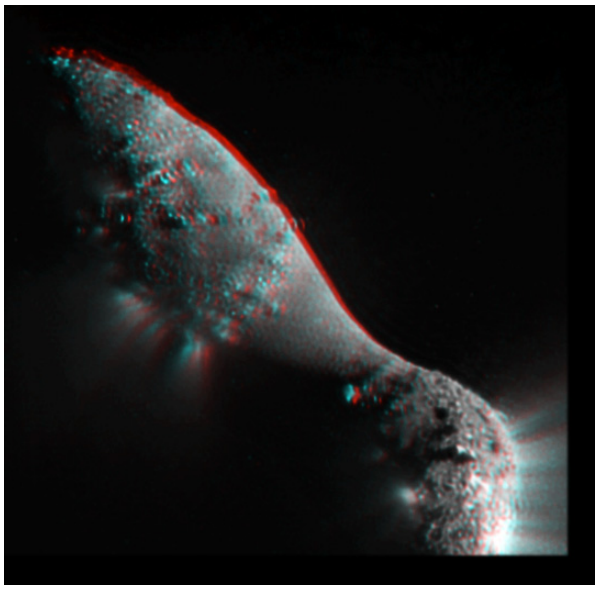

Fig. 2. Anaglyph version of the HRI-V image (HV10110414-5006007-001) taken on 4 November 2010 at a distance of 1820.2 km from the surface of 103P. The scale of the image is 3.64 m/px.

Once these features were manually identified in the high-resolution images, we measured their position on the surface of the comet, and assuming their shapes to be circumcircles, we derived their maximum length, that is the diameter, with the same methodology presented in Pajola et al. (2015); see Fig. 1. In addition, to obtain the cumulative boulder size-frequency distribution per km^2, we made use of the corresponding area computed from the 3D shape model of 103P by Thomas et al. (2013)[6].

For the specific case of boulders with sizes ≥30 m, we had the possibility of identifying not only the maximum length, called *a*, but we also measured the longest dimension perpendicular to this, called *b*. The aim of this approach is to determine the *b*/*a* ratio and compare that with the boulders studied on asteroids 25 143 Itokawa and 433 Eros, as in Michikami et al. (2010). This was only possible for boulders ≥30 m. As a result, in the case of smaller boulders, the ~3 m/px scale, coupled with the use of 103P deconvolved images (Lindler et al. 2013), makes the identification of the *b*/*a* ratio extremely difficult, and hence, only provides a confident measure of the maximum dimension of boulders.

3. Results

The global number of boulders identified on the illuminated side (~50%) of 103P is 400, 332 of which have diameters larger than

[6] The PDS reference for the shape model is: Farnham, T.L. and Thomas, P.C., PLATE SHAPE MODEL OF COMET 103PHARTLEY 2 V1.0, DIF-C-HRIV/MRI-5-HARTLEY2-SHAPE-V1.0, NASA Planetary Data System, 2013.

Table 1. The Deep Impact HRI-V images used in this work.

Name	Day	UT	Distance 103P center (km)	Scale (m/px)	Phase angle (°)	Solar elongation (°)
HV10110413-5004008-001-R	04-11-2010	13:57:20	1936.2	3.87	82.7	97.3
HV10110413-5004015-001-R	04-11-2010	13:58:07	1416.4	2.83	81.5	98.5
HV10110414-5006002-001-R	04-11-2010	14:01:26	1407.2	2.81	88.3	91.7
HV10110414-5006007-001-R	04-11-2010	14:02:03	1820.2	3.64	89.6	90.4

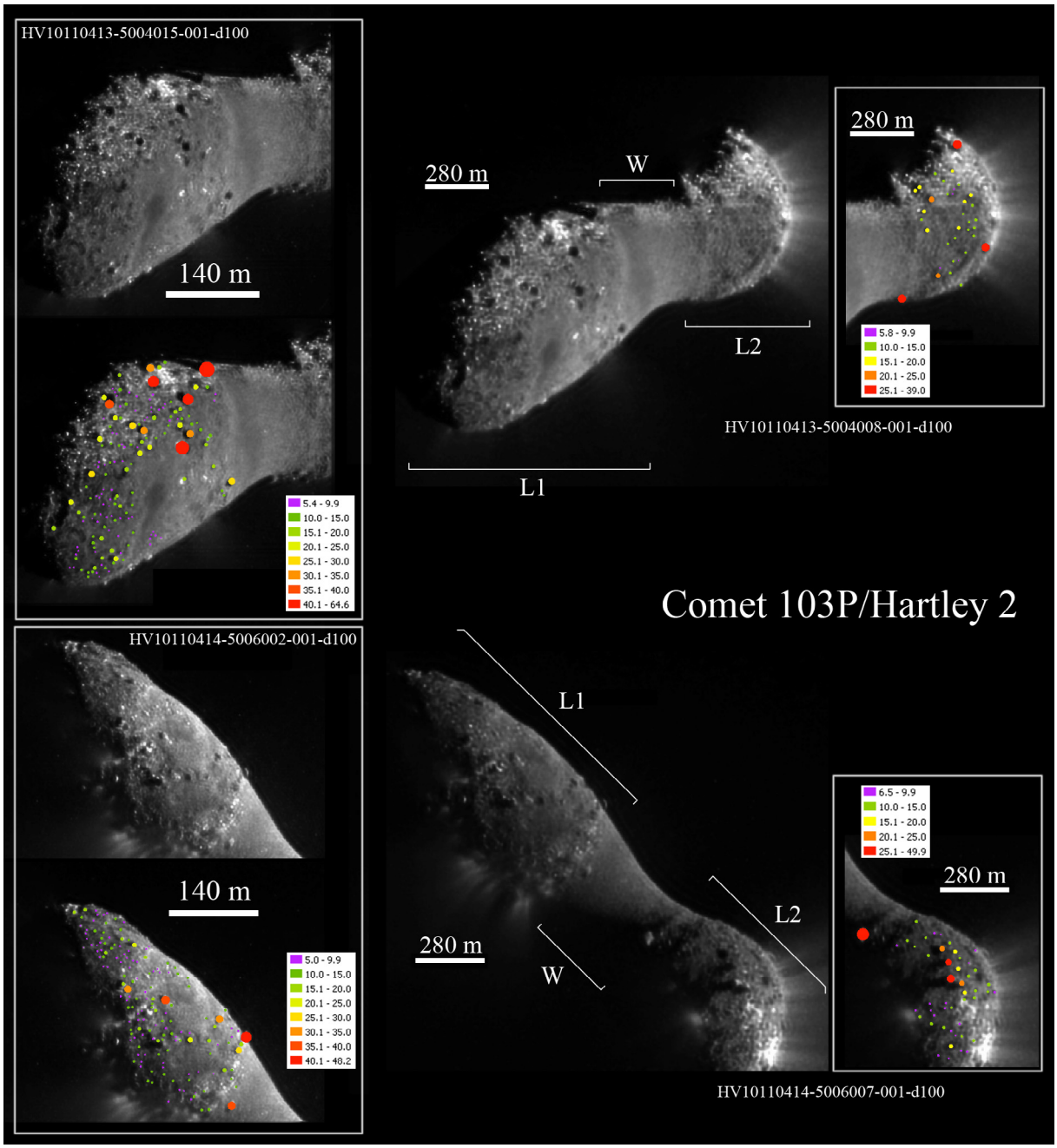

Fig. 3. Spatial distribution of the ≥10 m boulders on the illuminated side of 103P derived from HRI-V images (see Table 1 for image ID). The two lobes of the comet and the waist region are indicated with L1, L2, and W, respectively. Boulders smaller than 10 m in diameter are indicated in purple and are not considered in the size-frequency statistics.

10 m. Of the discarded 68 smaller boulders, 26 fall in the 9–10 m bin, 52 are between 8 m and 9 m, ten are between 7 m and 8 m, and the remaining six are inside the 6–7 m bin. Figure 3 shows the spatial distribution of boulders on 103P.

The cumulative boulder size-frequency distribution per km^2 of the entire illuminated side of the comet is presented in Fig. 4A, together with the histogram showing the normalized frequency of boulders ≥10 m present on the comet (Fig. 4B). The power-law index derived from the global boulder distribution is −2.7 ± 0.2. The regression line used to detect such index fits the binned values that are ≥10 m, but does not take those points that are equally cumulatively repeated above 38 m into

Table 2. Names of regions, their area from the 3D shape model (Thomas et al. 2013), the total number and surface density of boulders ≥10 m, power-law index, and associated error.

Name	$Area_{3D}$ (km^2)	Tot # boulders ≥10 m	# 10 m boulders per km^2	Power-index	+	−
All	2.38	332	140	−2.7	0.2	0.2
L1	1.24	258	208	−2.7	0.2	0.2
L2	0.67	74	111	−2.6	0.2	0.5

Notes. The 3D area of the illuminated waist region is 0.47 km^2.

account. The presence of the same cumulative number in subsequent values is an indicator of a poor statistics that does not have to be considered by the fit: such effect typically occurs at the bigger boulder sizes, as presented in Pajola et al. (2015) and Michikami et al. (2008). This is valid for all plots presented in this work. Moreover, we underline that when evenly spaced horizontal bins are considered for the fit in the logarithmic representation, no significant power-law index changes are present (they are well within the error bars here presented), hence, the 2 m bin size power-law indices can be considered a valid representation of the statistics. From Fig. 4B, we find that a non-negligible percentage of boulders (7%) is larger than 30 m with maximum sizes reaching 66 m in diameter. The maximum measured dimensions confirm the mound sizes presented in Fig. 5 of Thomas et al. (2013). In addition, by measuring the value of the observed area from the 3D shape model of Thomas et al. (2013) (the total observed illuminated side of 103P is 2.38 km^2, i.e., 45% of the total surface; see Table 2), we quantified a density of 140 boulders ≥10 m per km^2.

To see if any size-frequency distribution differences are present on the two lobes of 103P, we computed their power-law index with the same technique used for the global statistics. The lobe L1 has 317 boulders, 258 of which have a diameter ≥10 m, while L2 is characterized by 83 boulders, 74 of which are ≥10 m. The power-law index derived for L1 is −2.7 ± 0.2, while the one obtained on L2 is −2.6 +0.2/ − 0.5; see Fig. 5. The two lobes power-law indices completely overlap when taking the corresponding error bars into account. On the contrary, when considering the number of boulders ≥10 m per km^2, we derived that on L1 the number of boulders per unit area is almost double with respect to L2, i.e., 208 versus 111.

4. Analysis and discussion

4.1. The boulder size-frequency distribution analysis

The presence of boulders on the surface of 103P is a challenge in itself, since 103P is not characterized by cliffs or pits that could justify the occurrence of breakup and gravitational falls. Moreover, recent statistical studies have shown that even for Jupiter-family comets crossing the main belt every few years, the probability of an impact between an asteroid and a cometary nucleus is very low (Belton et al. 2013; Vincent et al. 2015), and hence the production of impact-related boulders is also low. As presented for 67P, (Pajola et al. 2015), another possibility that can explain the presence of boulders on the comet surface is the fact that at the time of comet formation, beyond the orbit of Neptune, the environment was much more favorable for collisions. Nonetheless, it is difficult to understand how boulders that were created 4.5 billion years ago can survive many perihelion passages and be observable now, when most of the comet surface has been heavily changed by activity. We therefore suggest that the boulders we see on the surface of 103P today may be, on the one hand, the results of fragmented outgassing surfaces and, on the other hand, possibly lifted chunks of surficial material that consequently fell back to the surface not having reached the escape velocity.

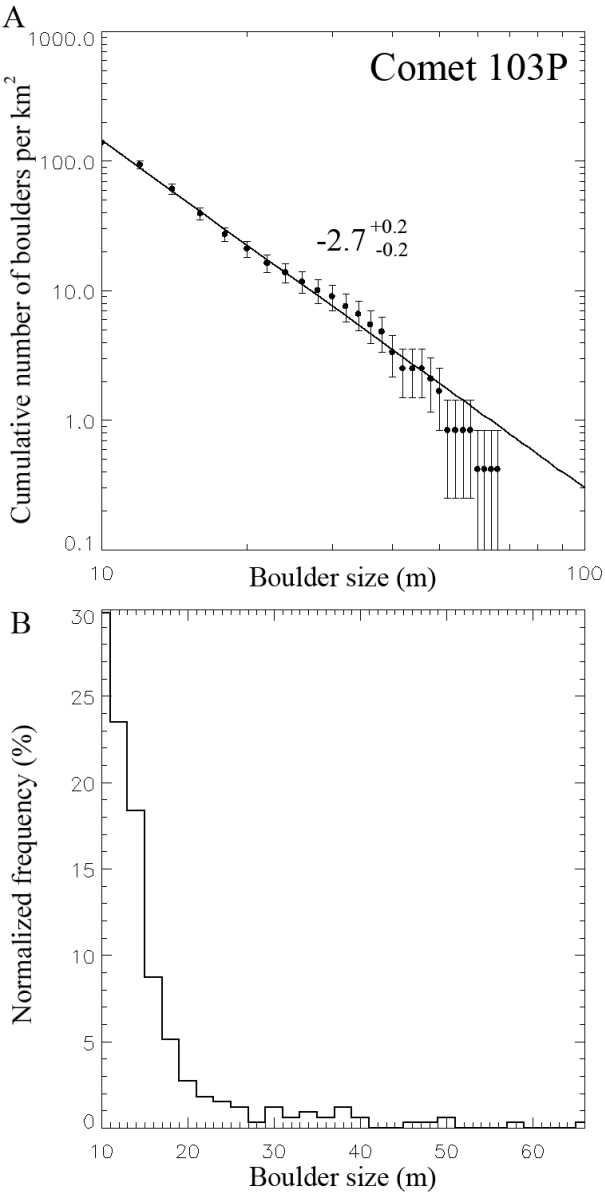

Fig. 4. **A)** Cumulative size-frequency distribution of boulders ≥10 m per km^2 over the illuminated surface of 103P (~50%). Vertical error bars indicate the root of the cumulative number of counting boulders, as from Michikami et al. (2008), divided by the illuminated area of 103P. The continuous line is a fitted regression line to the data, and the power-law index of the size distribution is −2.7 ± 0.2. The bin size is 2 m. **B)** Histogram presenting the normalized frequency in percentage per boulder size. As above, the bin here is 2 m.

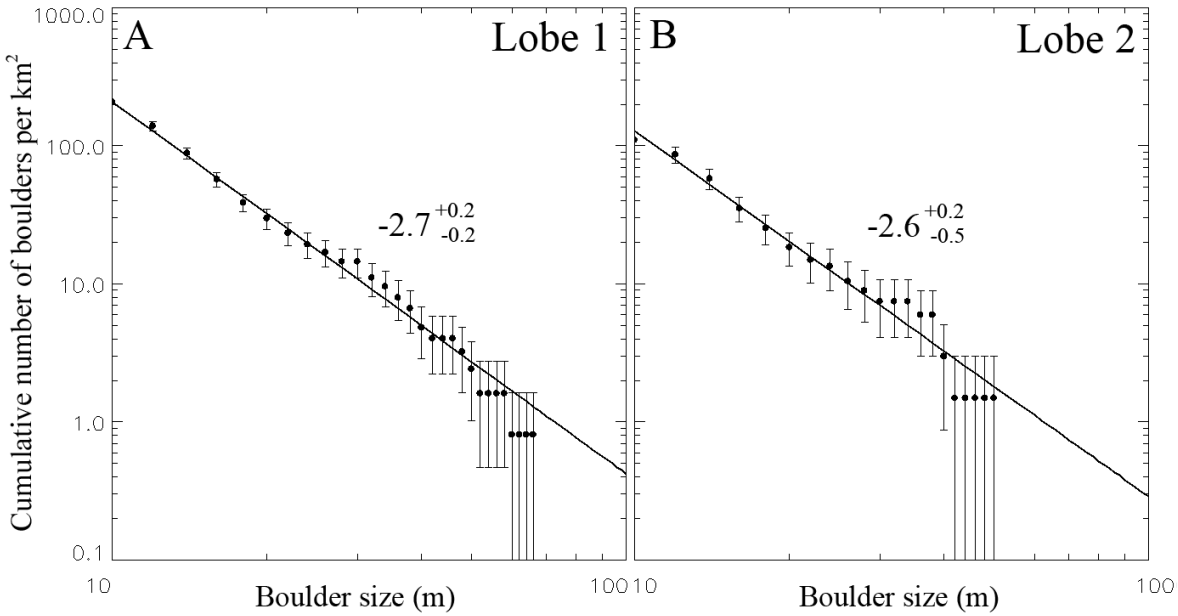

Fig. 5. Cumulative size-frequency distribution of ≥10 m boulders per km^2 of the two lobes, L1 and L2, of comet 103P. Vertical error bars are computed as Fig. 4. As for Fig. 4, the bin size here is 2 m.

As is clear from Fig. 3, boulders are ubiquitous on both rough lobes of the comet with the clear exception of the smooth waist region where no positive reliefs are present. A'Hearn et al. (2011) tentatively interpreted this region as a secondary deposit of material involving fallback of refractories and icy chunks from the two active lobes. This kind of interpretation could justify the absence of boulders in the connecting region that can be therefore completely buried below a thick layer of redeposited material. Two other concurring possibilities justify this absence of boulders. The past waist activity may have, on the one hand, completely fragmented and disintegrated the former boulders, leaving behind only a remnant dust blanket, and, on the other hand, it might be possible that the former boulders might have been lifted up from the surface of the comet though the outflowing gas exceeding local surficial gravity triggered by sublimation processes. According to the formulas described in Fulle (1997), large boulders would be lifted from the surface of 103P. Indeed, assuming a gas production rate of H_2O $Q \sim 1 \times 10^{28}$ s^{-1} (A'Hearn et al. 2011) and an expanding velocity in the range 500–1000 m s^{-1}, boulders as large as 50–180 m in diameter could be lifted from the surface by cometary activity. This would raise the question of whether the features interpreted as boulders are really blocks detached from the surface or superficial features of the comet. However, as explained by A'Hearn et al. (2011), 103P is an hyperactive comet, i.e., it produces more H_2O per unit time than should be possible by sublimation from the overall surface area of its nucleus. The super-volatiles, specifically CO_2, are the primary drivers of 103P activity dragging out chunks of nearly pure water-ice, which then sublime, and, hence, provide a large fraction of the total H_2O gaseous output of the comet. The active fraction of the mere nucleus is therefore necessarily much lower, hence, the maximum sizes of the liftable boulders have to be lower than the above value. A definitive size of the maximum liftable boulder is therefore difficult to estimate, however, the analysis presented in Kelley et al. (2013) indicates that at the time of the EPOXI closest approach, i.e., one week after 103P perihelion passage, the largest observed particles were reaching effective radii close to 4 m, and were not several decameters in size, as expected from the above computation. The 4 m size does not have to be considered the maximum liftable boulder size, which can be bigger, but instead, direct evidence that at least meter size boulders can be lifted.

The global size-frequency boulder distribution of 103P (Fig. 4A) shows a power-law index of -2.7 ± 0.2. If we compare these results with similar studies (Pajola et al. 2015) performed on 67P/Churyumov Gerasimenko (67P), it is derivable that 103P has a lower global power-law index, i.e., −2.7 vs. −3.6. In addition, the number density of boulders ≥10 m per km^2 on Hartley 2 is 4.4 bigger than on 67P (140 vs. 32). What does this mean? How can it be explained? As presented in Pajola et al. (2015), the global distribution of boulders of 67P is mostly dominated by boulders whose origin is related to gravitational events triggered by sublimation and/or thermal fracturing causing regressive erosion of pits and depressions. In the case of the illuminated side of 103P, these types of boulders cannot be proposed because no cliffs and walls are present. On the contrary, the possible power-law index similarity between 103P and the neck/Hapi of 67P (-2.2 ± 0.2) raise the question of whether there is a common or at least similar activity behavior occurring on such bodies.

Results by Sierks et al. (2015) indicate that the neck region of 67P was the most active area of the northern hemisphere, producing gas and dust jets and lifting dust grains. On the contrary, the hyperactivity of 103P works in a very different way than the normal activity of 67P in the neck/Hapi area. Indeed, the water of 103P-L2 is being carried out from below the surface as icy grains in the CO_2 jets, whereas the activity in Hapi is directly due to water sublimation, occurring below the surface and/or in the walls of cliffs and pits. For this reason, L2 of 103P and Hapi have very different physical processes going on, while L1 of 103P, presenting a much lower activity of CO_2, may be more similar to Hapi. Another possible explanation for the slightly steeper power-law index with respect to the size-frequency observed on the neck of 67P could be the absence of cliffs and walls on 103P (Thomas et al. 2013), which do not produce dusty material that might bury the smaller boulders by falling down the cliff. Therefore, the strong global differences in surface geomorphology and activity between 103P and 67P make them not easily comparable.

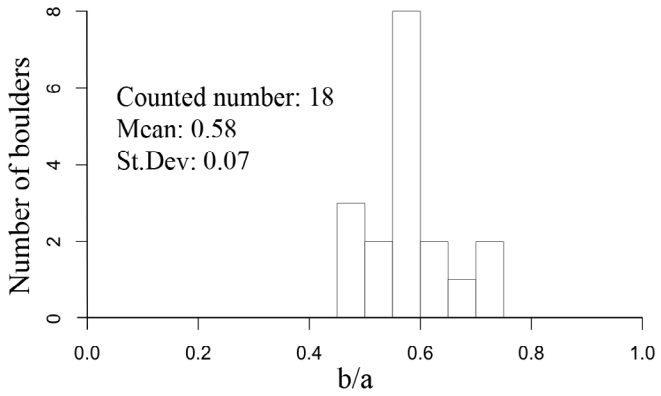

Fig. 6. Shape distributions of boulders ≥30 m on the surface of 103P. The horizontal axis shows the apparent axial ratio b/a of the boulders. The vertical axis shows the number of boulders.

By considering the two power-law indexes derived from the 103P lobes, we observe that despite a difference in the number density of boulders per km^2, they completely overlap (-2.7 ± 0.2 for L1 and -2.6 +0.2/−0.5 for L2) when taking the corresponding error bars into account. In addition, comparable maximum boulder sizes are present on both lobes. The most important consequences of these results are:

- The similar power-law indexes derived throughout the cumulative size-frequency statistics and the similar maximum boulder sizes between the two lobes both point toward a similar fracturing/disintegration phenomena of the boulders as well as similar lifting processes that may occur both in L1 and L2.
- The difference in number density per km^2, i.e., twice the boulders on L1 with respect to L2, suggest that the more diffuse H_2O sublimation on L1 produce much more boulders per km^2 with respect to those produced on L2, i.e., where the primary activity is CO_2 driven.

The proposed scenario for 103P boulders is that cometary outgassing from surficial fractures may lead to the residual features we see on the surface. Consequently, the widespread and strong activity (both H_2O and CO_2) of the hyperactive 103P might, on the one hand, completely disintegrate or fragment the smaller boulders making them disappear through sublimation. On the other hand, the smaller boulders might be lifted up by drag force produced by the outflowing gas triggered by sublimation processes and dispersed away from the comet into space (the lifting threshold depending on the boulder sizes). Such processes, as presented for 67P, both result in the decrease of smaller boulders with respect to larger boulders, and therefore lowering the cumulative size-frequency power-law index possibly to the value we see on 103P.

4.2. The shape distribution of boulders ≥30 m on 103P

On boulders ≥30 m, we had the possibility of measuring their maximum length, called a, as well as the longest dimension perpendicular to this, called b. We consequently determined the apparent b/a ratio of 18 boulders, 13 located on L1 and five located on L2. The mean apparent axial ratio, hereafter called b/a, measured on boulders with size of 30–66 m is 0.58, with a standard deviation of 0.07. The shape distribution of these kinds of boulders is presented in Fig. 6. If we compare the 103P b/a value with those derived by Michikami et al. (2010) on asteroids 25 143 Itokawa and 433 Eros, we see that the 103P value is closer to the Itokawa values than to those measured on Eros. Indeed, the b/a value of boulders ≥5 m on the entire surface of Itokawa is 0.62 with a standard deviation of 0.19, while the b/a value of boulders ≥4 m on Eros is 0.72. However, Itokawa b/a ratio can be traced back to that of collisional laboratory experiments and 433 Eros, i.e., 0.72, if regolith migration is invoked (Michikami et al. 2010). On the contrary, the 0.58 b/a value indicates that the 103P boulders ≥30 m are characterized by more elongated shapes compared with collisional laboratory fragments, therefore, suggesting a possible different origin. In addition, our 0.58 b/a value is also different with the value, 0.71, derived from small (<200 m) and fast (<1 h) rotating asteroids, which are considered to be preserved fragments produced by impact phenomena.

This analysis supports the interpretation that the cometary boulders of 103P, and cometary boulders in general, have a different origin[7] with respect to the asteroidal boulders, as confirmed by the above analysis on the size-frequency boulder distribution.

4.3. The comparison between 103P boulders and split fragments from cometary breakup events

An interesting comparison can be made between our −2.7 power-slope index measured on the size-frequency boulder distribution of 103P and the size-frequency distribution of fragments of split comets to see if there are any possible similarities. Indeed, more than 40 split comets have been observed in the past 150 years (Boehnhardt 2004) demonstrating that cometary breakups are not uncommon. In addition, depending on the type of cometary breakup, very few or several fragments may appear (Boehnhardt 2004), typically with subkilometer sizes (Lamy et al. 2004). What is truly challenging in these studies is to quantitatively derive the size-frequency distribution of the split fragments, since it is not unlikely that some of them behave as comets on their own with sublimating activity and dust production, the presence of a coma, and a tail.

Nonetheless, in few cases, such size-frequency distributions have been identified. Reach et al. (2009) studied the distribution and properties of fragments and debris from the split comet 73P/Schwassmann-Wachmann, hereafter 73P, via *Spitzer* data. Despite the difficulties in identifying the size-frequency distribution of 73P fragments, because many of them were actively emitting dust, Reach et al. (2009) find that the cumulative distribution of flux for these fragments has a slope of −0.42 for the small and −0.78 for the large fragments. As it is the flux proportional to the area, the size-frequency distribution of fragments has slopes of −0.84 and −1.56, respectively, i.e., significantly lower with respect to 103P −2.7 power-index. By switching to differential size-frequency distributions of −1.84 on 73P small fragments and −2.56 on 73P large fragments, Reach et al. (2009) compare 73P results with fragments of comet C/1999 S4 LINEAR (−2.72, as from Mäkinen et al. 2001), as well as with fragments derived from the Kreutz group of cometary Sungrazers (−2.7 to −3.0, as from Sekanina 2003), indicating how 73P fragments presents the shallowest power-index slope. Nevertheless, Ishiguro et al. (2009) used Subaru/Suprime-Cam data to derive a power-law index of the differential size distribution for 73P of −3.34, which

[7] In Sect. 2 of Pajola et al. (2015), multiple boulder formation processes are taken into account, such as fragmentation and sublimation, outbursts, and gravitational falls as well as lifting processes. An impact related origin is also evaluated in Pajola et al. (2015), but it is only presented as one of the multiple formation processes that can form and shape blocks in such changeable cometary surfaces.

is particularly higher with respect to Reach et al. (2009) measurements. This difference may be explained by the fact that the power index of these split fragments has large uncertainties associated with contaminations of dust grains surrounding these objects.

Our 103P cumulative power-index is −2.7, which is significantly steeper than the distribution of cometary fragments presented in Table 5 of Reach et al. (2009), indicating cumulative distributions slightly >−2.0. This seems to indicate that the processes of boulder formation on comets and comets breakups are different. Nonetheless, as for the case of 73P, the size distribution may evolve due to sublimation and are therefore lowered, as indicated by few fragments actively emitting dust.

For this reason, we believe that a definitive understanding of such processes requires, on the one hand, more global size-frequency boulders distributions of cometary nuclei (by taking into account this work, we have only two cometary global-size frequency distribution of boulders: one on 103P and one on 67P), as well as a wider database of the size-frequency distributions of cometary split fragments.

5. Conclusion

We presented the global size-frequency boulders distribution of comet 103P/ Hartley 2, measured on NASA EPOXI/HRI-V images of the nucleus. We derived the global size-frequency distribution of boulders larger than 10 m measured on the entire illuminated side of the nucleus (~50%), and subsequently focused on the different distributions of the two lobes that characterize the nucleus. The slope of the global size-frequency distribution shows a power-law index of −2.7 ± 0.2 and gives a density of 140 boulders ≥10 m per km^2. This trend can be justified by two concurring phenomena triggered by the widespread and strong activity of the hyperactive 103P comet: i) disintegration or fragmentation of the smaller boulders make them disappear through sublimation; and ii) lifting of the smaller boulders by drag force produced by the outflowing gas triggered by sublimation processes and dispersed away from the comet into space. Both processes result in the decrease of smaller boulders with respect to larger boulders, and, therefore, lowering the cumulative size-frequency power-law index possibly to the value we see on 103P.

The power-law indexes derived for the two 103P lobes (−2.7 ± 0.2 for L1 and −2.6 +0.2/−0.5 for L2) completely overlap. Despite a difference in the density of boulders per km^2, which suggest that the more diffuse H_2O sublimation on L1 produce twice the boulders per km^2 with respect to those produced on L2 (primary activity CO_2 driven), the similar power-law indexes and the similar maximum boulder sizes derived for the two lobes both point toward a similar fracturing/disintegration phenomena of the boulders as well as similar lifting processes that may occur both in L1 and L2.

When comparing the boulder distribution of the hyperactive 103P comet with similar studies performed on 67P (Pajola et al. 2015), it becomes clear that the 103P comet has a lower global power-law index (−2.7 vs. −3.6). The size-frequency boulder trend of 103P is somehow closer to the −2.2 value measured on the neck region of 67P, i.e., the most active region of the northern hemisphere of 67P (Sierks et al. 2015), but the hyperactivity of 103P works in a very different way than the normal activity of 67P in the neck/Hapi area. In addition to the global differences between the activities of the two comets, the absence of cliffs and walls on 103P shows a completely different surface geomorphology between Hartley 2 and 67P, thus, making them hardly comparable.

The study of the shape distribution of boulders ≥30 m performed on 103P suggests that the 103P boulders are characterized by more elongated shapes when compared to collisional laboratory fragments, as well as to asteroidal boulders, therefore, suggesting origins other than the impact related one.

The comparison between the boulder size-frequency distribution of 103P and the size-frequency distribution of fragments of split comets seems to indicate that the processes of boulder formation on comets and comets breakups are different. This is because cumulative size-frequency distributions of cometary fragments are slightly >−2.0, while our measured value on 103P is −2.7. Nonetheless, as for the case of 73P, the size-frequency distribution of fragments may evolve due to sublimation and is therefore lowered. Therefore, a definitive understanding of such processes requires, on the one hand, more global size-frequency boulders distributions of cometary nuclei (indeed, we only have two cometary global-size frequency distributions: one on 103P and one on 67P), as well as a wider database of the size-frequency distributions of cometary split fragments.

Acknowledgements. We thank the anonymous referee for important and constructive comments leading to great improvement of the paper. We made use of the public NASA-Planetary Data System images of comet 103P/Hartley 2. This research was supported in part by an appointment to the NASA Postdoctoral Program at Ames Research Center, administered by Oak Ridge Associated Universities through a contract with NASA. M. Pajola personally thanks Dr. Emanuele Simioni and Dr. Cristina Re for providing the values of the 3D surfaces of the illuminated sides of Hartley 2. M. A'Hearn acknowledges a Gauss Professorship from the Göttingen Academy of Science. We used both Arcgis 10.2 and IDL software to perform the presented analysis.

References

A'Hearn, M. F., Belton, M. J. S., Delamere, W. A., et al. 2005, Science, 310, 258
A'Hearn, M. F., Belton, M. J. S., Delamere, W. A., et al. 2011, Science, 332, 1396
Belton, M. J. S., Thomas, P., Carcich, B., et al. 2013, Icarus, 222, 477
Boehnhardt, H. 2004, Split comets, eds. M. C. Festou, H. U. Keller, & H. A. Weaver, 301
Fulle, M. 1997, A&A, 325, 1237
Harmon, J. K., Nolan, M. C., Howell, E. S., Giorgini, J. D., & Taylor, P. A. 2011, ApJ, 734, L2
Ishiguro, M., Usui, F., Sarugaku, Y., & Ueno, M. 2009, Icarus, 203, 560
Kelley, M. S., Lindler, D. J., Bodewits, D., et al. 2013, Icarus, 222, 634
Klaasen, K., A'Hearn, M. F., Baca, M., et al. 2008, Rev. Sci. Instrum., 79, 77
Lamy, P. L., Toth, I., Fernandez, Y. R., & Weaver, H. A. 2004, The sizes, shapes, albedos, and colors of cometary nuclei, eds. M. C. Festou, H. U. Keller, & H. A. Weaver, 223
Lindler, D. J., A'Hearn, M. F., Besse, S., et al. 2013, Icarus, 222, 571
Lisse, C. M., Fernandez, Y. R., Reach, W. T., et al. 2009, PASP, 121, 968
Mäkinen, J. T. T., Bertaux, J.-L., Combi, M. R., & Quémerais, E. 2001, Science, 292, 1326
Michikami, T., Nakamura, A. M., Hirata, N., et al. 2008, Earth Planets Space, 60, 13
Michikami, T., Nakamura, A. M., & Hirata, N. 2010, Icarus, 207, 277
Nyquist, H. 1928, Transactions of the American Institute of Electrical Engineers, 47, 617
Pajola, M., Vincent, J. B., Guettler, C., et al. 2015, A&A, 583, A17
Protopapa, S., Sunshine, J. M., Feaga, L. M., et al. 2014, Icarus, 238, 191
Reach, W. T., Vaubaillon, J., Kelley, M. S., Lisse, C. M., & Sykes, M. V. 2009, Icarus, 203, 571
Sekanina, Z. 2003, ApJ, 597, 1237
Sierks, H., Barbieri, C., Lamy, P. L., et al. 2015, Science, 347, aaa1044
Thomas, P. C., A'Hearn, M. F., Veverka, J., et al. 2013, Icarus, 222, 550
Vincent, J. B., Oklay, N., Marchi, S., Hoefner, S., & Sierks, H. 2015, Planet. Space Sci., 107, 53